JOURNAL OF PROPULSION AND POWER
Vol. 15, No. 4, July–August 1999

Hybrid Monte Carlo–Particle-in-Cell Simulation of an Ion Thruster Plume

Douglas B. VanGilder,* Gabriel I. Font,† and Iain D. Boyd‡
Cornell University, Ithaca, New York 14853

A numerical code is described that simulates the plumes of ion thrusters and Hall current thrusters. In the present study, computed flowfield results are compared with existing experimental measurements for the UK-10 ion thruster. The experimental measurements consist of ion flux, ion density, and floating potential data. The numerical code combines the direct simulation Monte Carlo method for modeling collisions with the particle-in-cell method for modeling plasma dynamics. Xenon neutrals and ions are modeled directly. Electrons are described by the Boltzmann relation. The effect of a finite back pressure experienced in laboratory experiments is included. Agreement between simulation and experiment is satisfactory. The simulation results are found to be very sensitive to input conditions assumed at the thruster exit plane. In particular, there is uncertainty in specifying the effects of the curvature of the dished grids of the UK-10 thruster on the ion exit velocity profile. The sensitivity of the simulations to certain model parameters is also examined. These include the cross section for charge-exchange reactions, the mechanics of charge-exchange reactions, and the electron temperature. The beam ions are found to be only moderately dependent on these variations, whereas the charge-exchange ions are sensitive to them.

Introduction

IT is necessary to understand the plumes of spacecraft propulsion systems for the assessment of spacecraft impingement and contamination issues. The plume divergence angle for impingement and the charge-exchange plasma for contamination by heavy metallic ions are of particular concern for ion thrusters and Hall current thrusters (HCTs). In these devices, not all of the atoms are ionized before exiting the thruster. Therefore, these neutrals close to the thruster, having thermal velocities, may collide with ions. Some of these collisions lead to charge-exchange interactions, in which an electron is transferred from the neutral to the ion. This process forms highly energetic neutrals and ions with thermal speeds. These slow ions may interact with conducting surfaces on the spacecraft, possibly altering the surface properties. On ion thrusters, they may be pulled back by the potential grids, causing grid erosion. The charge-exchange plasma leads to spreading of the beam and to acceleration of heavy metallic ions into the plume backflow region. The behavior of charge-exchange ions is therefore of particular interest. Computational modeling allows the dynamics of the plume and its interaction with its environment to be examined. The ability to simulate the plumes of these devices permits a wider variety of operating conditions to be tested and also eliminates the influence of the experimental facilities. The goal of the present study is to establish the aspects of the modeling that are significant in defining the plume profile. To validate the computer-modeling capabilities requires experimental data.

A hybrid direct simulation Monte Carlo[1]–particle-in-cell[2] (DSMC–PIC) code is being developed to understand, in detail, the plasma behavior of the plumes of ion thrusters and HCTs. The PIC method determines the trajectories of charged particles as predicted by imposed and self-consistent electric fields. The DSMC method is used to deal with the collisional effects in the flowfield. Both charge-exchange and momentum transfer collisions are modeled. The code is tested on the UK-10 thruster using xenon as a propellant, because of the availability of experimental data. The UK-10 is an electron bombardment ion thruster with a 10-cm nozzle exit diameter.[3] The acceleration grids are dished inward to focus the ion beam and diminish the beam divergence. Concave curvature allows the intergrid region to expand when the grids heat up, reducing the possibility of arcing. The simulation results are compared with measurements of ion flux and floating potential by de Boer,[4] and to measurements of ion density obtained by Pollard.[5] To model the thruster plume, assumptions are made to address physical uncertainties. Among these are the cross sections for charge-exchange reactions, the mechanics of the charge-exchange reactions, and the electron temperature. The sensitivity of the charge-exchange ion profile to these assumptions is examined.

The numerical method is described in the next section. This is followed by a discussion of both the comparison of simulation results with experiment and the sensitivity study. The paper closes with some brief conclusions.

Numerical Method

There are several issues that need to be addressed to simulate the plumes of ion thrusters. Computational grids must be generated, based on disparate length scales that describe the plasma and collision phenomena. Appropriate boundary conditions for the electric field must be imposed. The behavior of the charge-exchange ions is determined by the beam ions, neutrals, electric fields, and collision dynamics. The following subsections describe the important aspects of the present implementation.

Neutrals

Earlier work by Roy[6] employed the PIC method to model ion thruster plumes. Wang et al.[7] modeled ion thrusters using a PIC–Monte Carlo collision (MCC) algorithm. Each of these studies used an analytical expression to specify the spatial distribution of neutral atoms. A source term was then used for the charge-exchange ions, based on an analytical production rate. The current DSMC–PIC code tracks the neutrals (and their properties) as well as the ions. Charge-exchange ions are generated directly from collisions between neutral atoms and ions. By including the neutrals as particles, their velocity distribution is better represented. The fast neutrals created by charge-exchange would be absent from the analytic representation. Without these fast neutrals, the density would be overpredicted. The probability of charge-exchange is based on the relative velocity through the collision cross section given by Rapp and Francis.[8] Experimental work by Pollard[9] suggests a

Received 21 November 1997; revision received 10 August 1998; accepted for publication 26 September 1998.

*Graduate Student, Mechanical and Aerospace Engineering, Upson Hall.
†Postdoctoral Research Associate, Mechanical and Aerospace Engineering, Upson Hall.
‡Associate Professor, Mechanical and Aerospace Engineering, Upson Hall. Member AIAA.

charge-exchangecross section for xenon, which is 3–8 times higher than this theory predicts. This would lead to a higher production rate of charge-exchange ions. A test case assuming the theoretical value is compared with a case using three times this value for the cross section.

Propellant utilization efficiencies for ion thrusters are generally well above 50%. Because of their very low velocities, however, the density of the neutrals is higher than the ion density at the thruster exit. Therefore, the behavior of these neutrals determines the rate and location of the charge-exchangereactions. The charge-exchange production rate is linearly dependent on the neutral density. Sonic conditions for the neutrals are assumed at the thruster exit, based on a stagnation temperature of 500 K. A related study[10] demonstrates that the assumption of sonic flow agrees well with experiments of neutral xenon flows. It also compares the resulting neutral profile with that given by the analytical model assumed by Roy.[6] Lower neutral densities are predicted by these simulations.

Background Gas

Ground-based experiments have a finite ground pressure determined by the capacity of the pumping system. Although this usually gives a density well below the exit density of the neutrals, the two values become comparable in the near plume. Thus, the background density must be included in the simulations. It is assumed to be composed entirely of xenon neutrals, because the beam ions are moving at much higher velocities, and thus, leave the domain more easily. These neutrals collide with ions and neutrals that originate from the thruster. The background particles are not simulated directly, because it is not necessary to update their positions or know their exact properties. Instead, in each computational cell, temporary particles are created every time step with velocities sampled from a Maxwellian distribution at 295 K. The background density is assumed to be uniform. This is reasonable away from the thruster where its effects are as significant as the foreground neutrals. It is not necessary to model collisions between pairs of background atoms. It is assumed that the background distribution is unchanged with collisions. This assumption is reasonable, because the largest change would be a result of the fast atoms created by charge-exchange reactions. The magnitude of their density is about three orders of magnitude below the total background density for the case under consideration.

Charged Particles

The PIC algorithm uses charged particles and determines the charge density at the nodes of the grid cell, based on the proximity of each particle to the surrounding nodes. The scheme developed by Ruyten[11] has been shown to conserve charge density as well as charge. The charge density is then used to calculate the potential at the nodes. By keeping only the dominant terms of the electron momentum equation and assuming isothermal electrons, the electron density can be described by the Boltzmann relationship:

$$n_e = n_{\text{ref}} \exp(e\chi / kT_e)$$

where n_e is the electron density, e is the electron charge, χ is the potential, k is the Boltzmann constant, and T_e is the electron temperature. This is valid for a collisionless, isothermal plasma, where the gradients in potential are caused by gradients in density and magnetic field effects are negligible. Because magnetic forces in the plumes of ion thrusters are small compared with electrostatic forces, their effects can be ignored.

The difference in magnitudes of the ion and electron velocities makes it difficult to include the electrons as particles in the simulation. Moreover, it is the ion behavior that is of interest. By assuming that the plasma is quasineutral ($n_i \approx n_e$), the ion density can be used to find the potential, and the electrons need not be tracked. Based on measurements of floating potential and electron energy in the plume of the UK-10 ion thruster, de Boer[4] estimated the degree of nonneutralization $[(n_i - n_e)/n_e]$. In the beam region, it is estimated to be on the order of $10^{-5}-10^{-4}$.

To find the potential, a value for the electron temperature is required. Experimental work with the UK-10 ion thruster[4] gives a value ranging from 0.5 to 3.0 eV, depending on where in the flowfield it is measured. A value of 1.0 eV is chosen for most of these simulations, and is compared with a test case with $T_e = 5.0$ eV to examine the sensitivity. For the plasma to be collisionless with respect to Coulombic collisions, the ratio of collision frequency to ion plasma frequency is considered. This is

$$\nu_{ei} / \omega_{pi} \approx \ell n N_D / N_D$$

where N_D is the number of charged particles in a Debye cube, and ν_{ei} is the electron–ion collision frequency.[6] This ratio ranges from 1.7×10^{-3} for 1.0 eV to 1.9×10^{-4} for 5.0 eV, based on the average ion density at the thruster exit. Also, $\nu_{ee} \approx \nu_{ei}$ and $\nu_{ii} < \nu_{ei}$ unless $T_e \gg T_i$; therefore, this ratio gives a reasonable estimate for Coulombic collisions. Because these ratios are much less than 1 in the present study, it is reasonable to consider the plasma to be collisionless.

Experiments have shown that the plume of ion thrusters is composed of 5–15% doubly charged ions and trace fractions of ions with greater charge.[5,12] The ions are assumed to be singly charged, although the code is capable of handling these multiply charged ions. To examine the behavior of the charge-exchange ions separate from the beam ions, they are treated as different species in the code.

Collision Dynamics

Charge-exchangereactions can occur when a highly energetic ion collides with a neutral atom at a thermal speed. A slow ion and a fast neutral are the result of this reaction, but the exact postcollisional properties are not clearly defined. To capture this behavior, the simulated particles in the collision merely exchange an electron and maintain their precollision velocities. Although physically, there would be a momentum change, the extent to which the paths are altered is unknown. This method is compared with one in which elastic hard-sphere collisions are assumed and the momentum is transferred between particles. In this case, the scattering angle is chosen randomly from an isotropic distribution as is done with the noncharge-exchange collisions. These collisions use the variable hard-sphere model.[1]

Grids

The length scale for which a plasma can be treated on a particle level is given by the Debye length. This length is generally used to scale the computational grid cells in PIC simulations. Grid cells used for DSMC are generally scaled by the mean free path, the length scale for collisions. Both lengths are functions of density. For the properties of ion thrusters, the Debye length is usually much smaller than the mean free path. Therefore, two different grids are employed by the code. There is no interaction between the two grids. The underlying DSMC code (MONACO[13]) is capable of handling the unstructured grids, whereas the PIC part of the code uses nonuniform regular grids. Memory may become an issue with two grids modeling a large domain. Therefore, the PIC grid is implemented implicitly. The only values necessary for each node of the cells are its potential and its electric field vector. The positions of the nodes are stored implicitly in two one-dimensional arrays, rather than in a two-dimensional array. This modification does not affect the computational time significantly, but can save a substantial amount of memory. Figure 1 shows the two grids used for the simulations. The upper one is the DSMC grid, and the lower one is the PIC grid.

Boundary Conditions

The exit plane of the ion thruster has a physically imposed boundary condition given by the potential of the accelerator grid. The nodes of the PIC grid that lie on the exit plane of the thruster have a potential given by the sum of the accelerator grid's potential and the contribution of the nearby ions. The wall of the thruster is assumed to be biased to the spacecraft potential, which is estimated to be

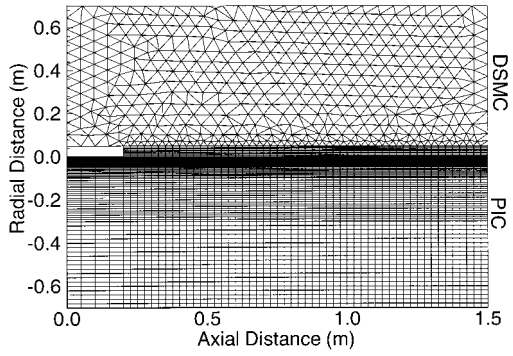

Fig. 1 Computational grids.

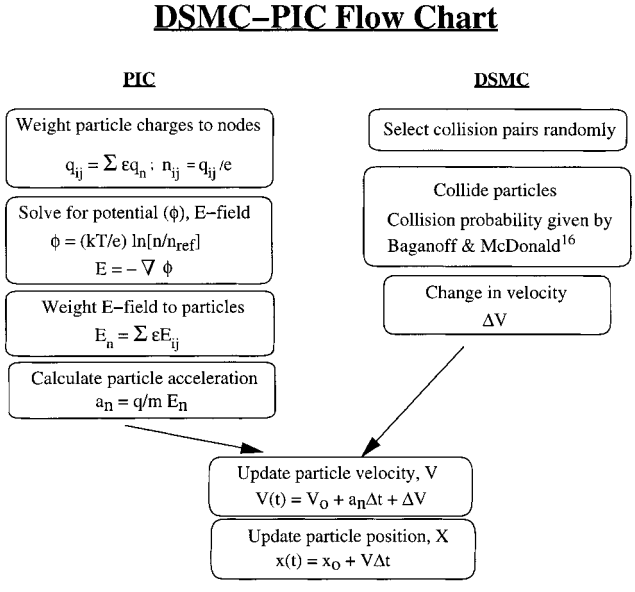

Fig. 2 One time step of algorithm.

kT_e/e.[6] The reference density defined at a location where the potential is set to zero (n_{ref}) is needed for the Boltzmann relationship to obtain the potential. This value is obtained by matching the ion density at the thruster exit nearest the axis with an extrapolation of the potential measurements taken along the axis by de Boer.[4] To prevent the potential from going to $-\infty$, when no ions are in a PIC cell, a small perturbation is introduced. A value is added to the term inside the logarithm. Effectively, this gives a lower bound on the potential.

Experimental results of ion thrusters suggest a Gaussian distribution of current density.[4,12] Therefore, the Gaussian ion density profile assumed by Wang et al.[7] is used at the exit plane. The UK-10 ion thruster has both the screen grid and the accelerator grid dished inward to provide mechanical stability and to reduce beam divergence.[3] The extent to which this curvature affects the exit profile of the ions is unknown. Its effect on the atoms is assumed to be negligible. By using a dishing depth of 5 mm, various exit profiles are tested.

The domain is assumed to be axisymmetric about the thruster centerline. The main three-dimensional effects would come from the location of the neutralizer, but the quasineutrality assumption makes these effects negligible. Near the thruster exit, the electrons from the neutralizer are not sufficient for neutrality. The large electric field this leaves is given by the accelerator grid potential boundary condition. The radial electric field is set to zero on the centerline to satisfy symmetry, but axial variations in potential are permitted. The upper boundary also allows only axial variations in potential. The other two boundaries allow radial, but not axial, variations in potential. This assumption is valid when the domain is sufficiently large. Particles that reach boundaries other than the symmetry line leave the simulation.

Integration of the Two Particle Methods

The DSMC and PIC methods are compatible because they require very little interaction. The collisions are handled by the DSMC algorithms, as are the updating of particle positions and the output of macroscopic variables. The PIC algorithms determine the electric field vector from the potentials at the nodes. The change in particle velocities caused by this electric field is then combined with changes caused by any collision, to update the velocities and then the positions. The initial properties of the particles are based on a specified distribution function. Work by Oh and Hastings[14] combined PIC and DSMC to simulate Hall thruster plumes. Gatsonis and Yin[15] simulated pulsed plasma thrusters that use ablated Teflon as propellant with a similar algorithm. The present application to xenon ion thrusters relies on experimental evidence to address physical modeling issues. Figure 2 shows a flow chart of the algorithm used here over one time step. The collision algorithm is based on the scheme proposed by Baganoff and McDonald.[16]

The main incompatibility is because of scale length discrepancies. As mentioned earlier, two separate grids can be easily maintained by this implementation. This leads to two problems. First, for reasonable statistics, the PIC method needs about 10 ions per cell. This leads to the use of a larger number of particles per DSMC cell than is usually needed. Over 1000 particles, including atoms, are used in some cells. The other issue is the time scale. For both methods it is desirable to have a particle remain in a cell for a few time steps. Fortunately, the gradients in ion density in the axial direction are less pronounced than in the radial direction, and the ions are moving predominantly in the axial direction. This allows larger axial PIC cell lengths, so that the time scales for the two grids agree. The time scale of choice is the inverse of the ion plasma frequency, the frequency at which the ions oscillate about their equilibrium positions. Because this value is considerably less than the collision time scale, very few collisions are computed each time step.

Results and Discussion

The conditions specified for the simulations are flow rate ($\dot{m} =$ 0.73 mg/s), thrust (18 mN), beam current (0.33 A), and beam voltage (1100 V). The back pressure in the vacuum tank is assumed to be 2×10^{-6} torr. The computational domain is composed of 1400 DSMC cells and 3900 PIC cells. It extends 1.3 m axially and 0.7 m radially from the thruster exit. Inside the ion beam, the nodes of the DSMC cells coincide with nodes of the PIC grid. The execution time is about 48 h for a 500,000 particle simulation on an R10000 SGI workstation.

The aforementioned Gaussian density profile is combined with a uniform ion velocity of 40 km/s at the exit, as predicted by a voltage drop of 1100 V. This base case is used as a starting point to test the behavior of the code. Further assumptions include an electron temperature of 1.0 eV and the theoretical charge-exchange cross section with no momentum transfer for charge-exchange collisions. Figure 3 shows the ion flux vs radial position at various axial locations. The shape of the profile is maintained throughout the region,

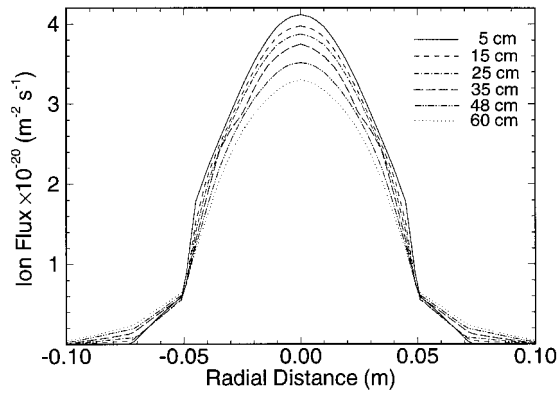

Fig. 3 Radial profiles of ion flux at various axial locations for base case.

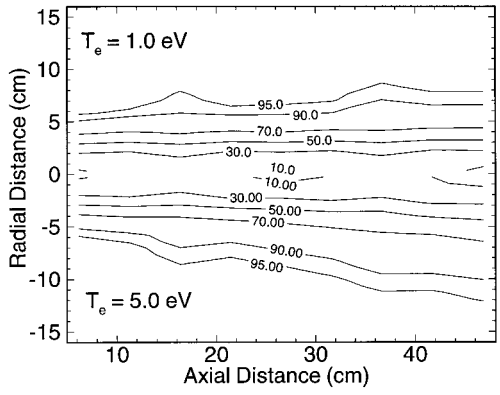

Fig. 4 Integral flux contours for both electron temperatures.

but the magnitude at the centerline decreases along the axis, as the beam spreads. Figure 4 shows this contour given as the percentage of ion current enclosed below the radial position, and a comparison with the case with an electron temperature of 5.0 eV. Comparing the two shows that the ion temperature is not the only cause of spreading. The potential gradients are magnified by a larger electron temperature for similar density gradients.

These results are not surprising if one considers the magnitude of the electrostatic forces compared with the hydrodynamic forces. As the ion beam passes through a cell in the computational domain, it experiences an electrostatic force in the radial direction, because the gradients in density are steepest in that direction. The ratio of this to the axially directed force should give a measure of the amount of spreading of the beam across a cell. The electrostatic force across a cell is

$$F_E = NqE = Nq(\Delta\chi/\Delta y)$$

where $\Delta\chi$ is the change in potential, and Δy is the radial grid node spacing. Here, N is the number of ions in the volume represented by the cell, q is the charge of an ion (+e), and E is the electric field magnitude. The hydrodynamic force is

$$F_{mv} = \dot{m}u_x = \rho uAu = \bar{n}mu_x^2 A$$

where $\dot{m}$ is the flow rate, and u_x is the axial velocity. The area A is of the cell face, ρ is the mass density, $\bar{n}$ is the average ion number density, and m is the mass of an ion. The ratio of the two is given by

$$\frac{F_E}{F_{mv}} = \frac{Nq\Delta\chi}{\bar{n}mu_x^2 A\Delta y} = \frac{q\Delta\chi}{mu_x^2(\Delta y/\Delta x)}$$

Because q and m are known, and assuming that $u_x \approx 35$ km/s caused by deceleration close to the grid, this gives a value of 6×10^{-4} $[\Delta\chi/(\Delta y/\Delta x)]$. This indicates that the bending of the beam is only significant for large changes in potential across the cell. Using the Boltzmann relationship, the change in potential varies as $T_e \ln(n_2/n_1)$, where n_1 is the ion density at the lower node, and n_2 is the ion density at the upper node. Inside the beam, this density ratio is between 1 and 5, which would not make a very significant potential difference. With a higher electron temperature, the spreading is more pronounced.

The uniform velocity case is run with and without back pressure. Figure 5 shows the contours of the density of the charge-exchange ions for the two cases. In both cases, it is clear that their production is significant. Ions spread as a result of electric fields. These forces are strongest on the edge of the beam where density gradients are largest. The beam ions are moving so quickly in the axial direction that they are not affected as much as the charge-exchange ions. The electrostatic forces pull these charge-exchange ions away from the beam. This is most apparent near the thruster exit, where most of the charge-exchange reactions take place. These ions are pulled away from the beam before they spread too much thermally. This explains the lobe a few centimeters from the exit, close to the beam. Also, the uniform contours above the beam are not what would be expected

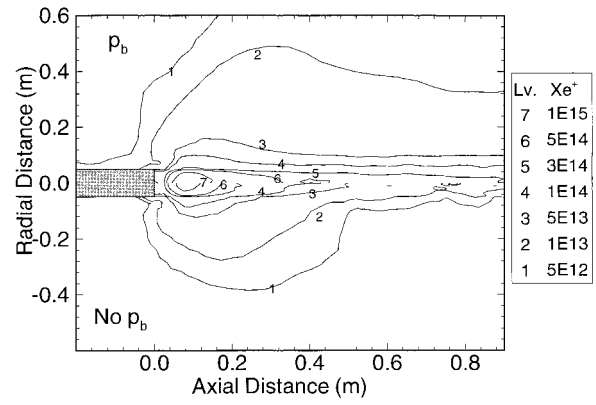

Fig. 5 Contours of charge-exchange ions for uniform velocity case with and without back pressure.

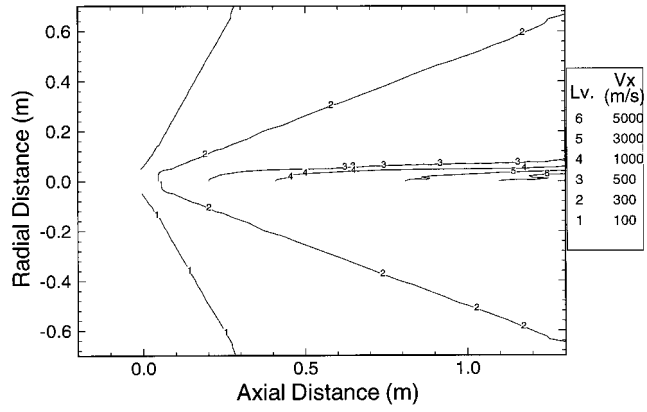

Fig. 6 Contours of average axial velocity of thruster neutrals with and without ions.

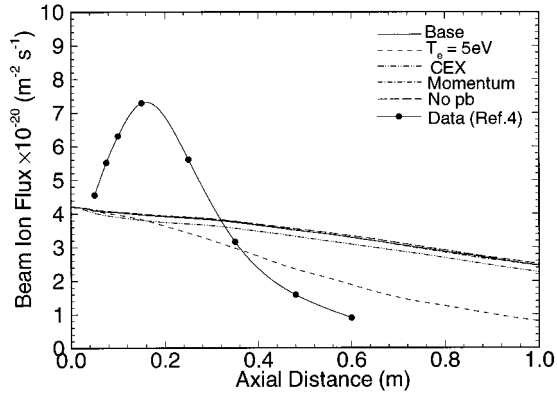

Fig. 7 Comparisons of ion flux along axis for various cases.

from thermally spreading ions. Near the axis, the ion flux is given by the beam ions. The effects of back pressure on the magnitude and location of the charge-exchange ions are significant. Their density is lower along the axis without the back pressure, because very few charge-exchange reactions take place in the far plume. Also, less charge-exchange ions reach the region behind the thruster exit.

Figure 6 shows the influence of the creation of fast neutrals on the distribution of thruster neutrals. It is a plot of the average axial velocity of the thruster neutrals. The lower half is without ions, and the upper half includes the fast neutrals. The increase in average velocity indicates that a substantial fraction of the neutrals have undergone a charge-exchange reaction. A comparison of neutral density shows a corresponding decrease for the case with ions, but the effect is less pronounced.

Figure 7 shows the flux along the axis for the variations of the base case. Base indicates the base case described earlier, CEX indicates

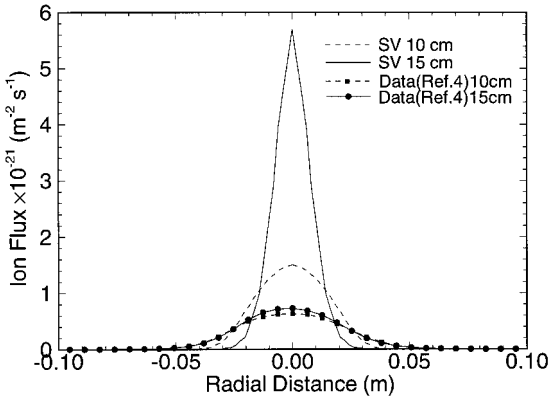

Fig. 8 Comparisons of SV test case with ion flux from experiment 10 and 15 cm from the exit.

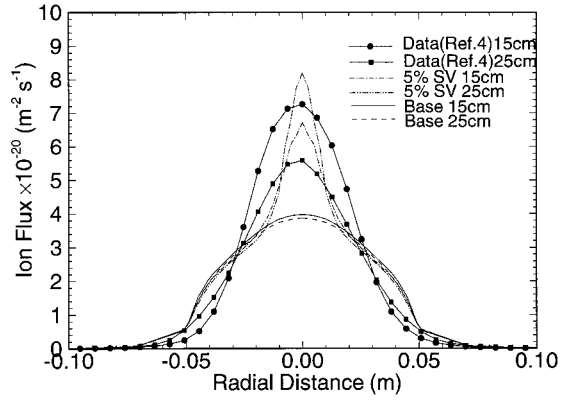

Fig. 9 Comparisons of ion flux from various ion velocity profiles to experiment 15 and 25 cm from the exit.

the case where the charge-exchange cross section was increased, Momentum indicates full momentum transfer for charge-exchange reactions, No p_b is without back pressure, and $T = 5$ eV is the higher electron temperature case. As this figure shows, the experiment indicates a peak in flux along the centerline near 15 cm from the exit because of the focusing of the curved grids. In fact, there is a waist found experimentally[4] at this location. It is clear that none of these cases captures the observed behavior. A uniform velocity profile does not take into consideration the effect of the accelerator grid curvature. To account for the focusing, the dish is assumed to be spherical, which, together with the dish depth of 5 mm, specifies the focal point at 25.25 cm from the thruster exit. By assuming that the ion bulk velocity vector at the thruster exit is perpendicular to a spherical accelerator grid, a spherical velocity (SV) profile is defined, which focuses the beam at this focal point. Use of this SV profile in a simulation provides a peak ion flux at the focal point that is well above that of the experiment, and is therefore not shown in Fig. 7. The location of the peak falls about 5 cm short of the focal point because of deceleration of the beam caused by the grid potential boundary condition. A test case that assumes a parabolic dish gives similar results. Comparisons between the simulation that assumes the SV profile and ion flux measurements at two axial locations near the waist of the beam are shown in Fig. 8. The sharp peaks near the axis indicate that the focusing of the thruster grid is much less pronounced than a fully spherical grid predicts. In this case, as well as the parabolic profile case, the bulk of the ions reach the axis, and the waist is therefore very narrow. Hence, it is concluded that the paths of the ions are not determined exactly by the dish geometry.

The true profile must lie somewhere between this and a uniform velocity profile that provides no focusing. To help quantify the departure from full focusing, the spherical and uniform velocity profiles are superimposed. Mixed profiles of 5% spherical, 95% uniform velocity and 10% spherical, 90% uniform velocity are each employed. The 5% case agrees well with the magnitude of the experimental flux (see Fig. 9), but it too has a very pronounced peak. Figure 9 also shows that the uniform velocity case agrees well in shape with the experiment. Figure 10 shows good agreement for all cases with the experiment 5 cm axially from the thruster exit. Therefore, the inlet ion profiles tested are not unreasonable. These simulations demonstrate that the beam essentially follows its initial velocity profile, as predicted by the ratio of electrostatic to hydrodynamic forces.

Pollard[5] measured ion density in the plume at various angles at fixed distances from the exit using a Langmuir probe for a slightly higher thrust (20 mN). Comparisons of ion density 30 cm from the thruster exit between various uniform velocity simulations and these data are presented in Fig. 11. Qualitatively, the simulation results agree quite well with the measured data.

Figures 12 and 13 show comparisons at 61 and 122 cm, respectively, from the exit. In each case, the uniform velocity profiles overpredict the ion density near the axis. Consistent with these peaks,

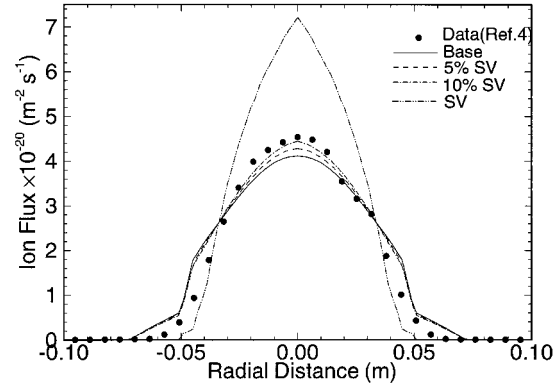

Fig. 10 Comparisons of ion flux from various ion velocity profiles to experiment 5 cm from the exit.

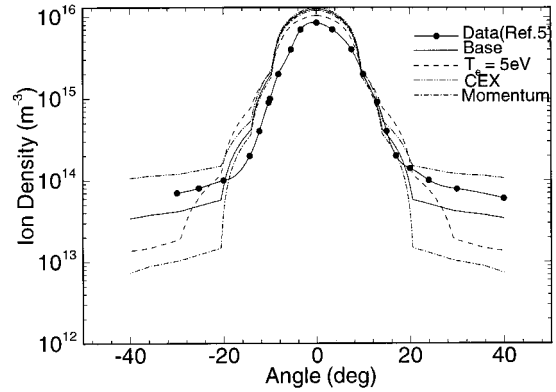

Fig. 11 Comparisons of ion density to experimental measurements by Pollard[5] taken at various angles 30 cm from the center of the exit.

the experiment shows more spreading at large angles away from the axis. The effect on the charge-exchange ions is apparent in these plots. They dominate the ion density away from the beam in the wings of the profiles. As expected, the ion density is highest for the case with a larger charge-exchange cross section (CEX). This case and the base case agree better at these locations with the experiment. The momentum transfer case predicts a lower density, because the postcollisional velocity of the charge-exchange ions is substantially higher for this type of collision. The larger electron temperature predicts more beam spreading (as seen in Fig. 4), but the agreement with ion density is not as good. These ion density comparisons and Fig. 7 indicate that the beam ions are only slightly affected by changing these physical parameters.

Figure 14 shows a typical result for the beam ion flux for the different uniform velocity cases. The momentum transfer case is

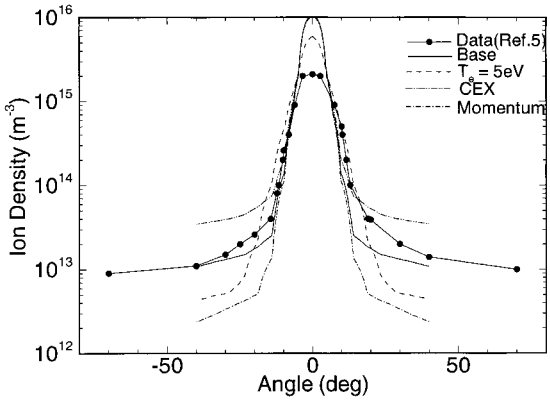

Fig. 12 Comparisons of ion density to experimental measurements taken at various angles 61 cm from the center of the exit.

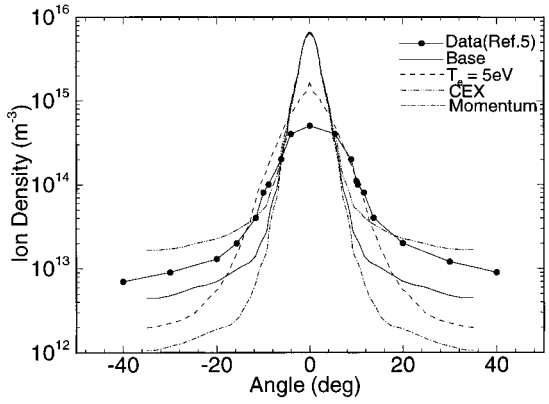

Fig. 13 Comparisons of ion density to experimental measurements taken at various angles 122 cm from the center of the exit.

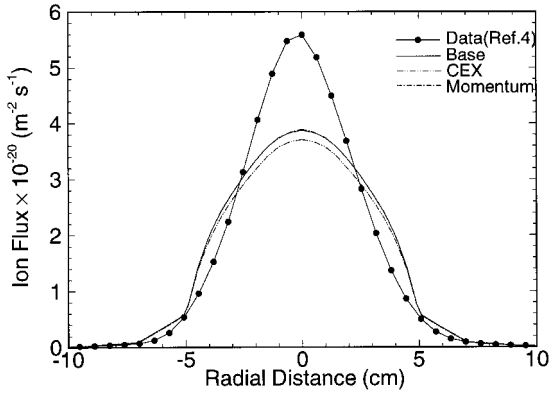

Fig. 14 Comparisons of ion flux 25 cm from the thruster exit for various uniform velocity cases.

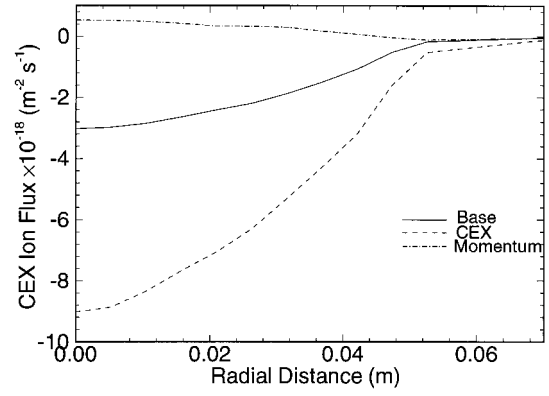

Fig. 15 Comparisons of charge-exchange ion flux at the thruster exit for various uniform velocity cases.

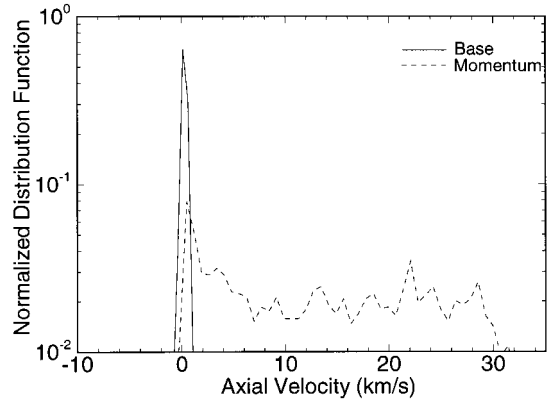

Fig. 16 Normalized axial velocity distribution functions of charge-exchange ions at the beam edge (r = 5 cm), 10 cm away from the thruster exit plane.

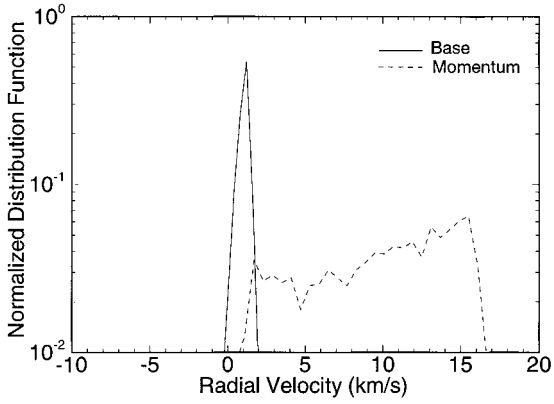

Fig. 17 Normalized radial velocity distribution functions of charge-exchange ions at the beam edge (r = 5 cm), 10 cm away from the thruster exit plane.

nearly identical to the base case, because the depletion of the beam ions by charge-exchange reactions is unaltered. The cross-section case is only slightly lower because of a higher charge-exchange collision rate. Closer to the exit, the difference is even less. As with the ion density comparisons, this indicates that the ion beam is insignificantly changed by these parameters. However, subsequent plots will show how the charge-exchange ion profile is affected.

Figure 15 illustrates the differences in charge-exchange ion flux near the exit. It is clear that the experimentally measured flux is almost entirely beam ions, because the charge-exchange ion flux is two orders of magnitude below that of the beam ions. The behavior of the charge-exchange ions near the thruster is of particular interest. It is these ions that may be pulled back by the grid's potential, and impinge on its surface. This may cause sputtering of grid material. The base case and the cross-section case both show a flux of ions back into the grid. Thermal velocities are not strong enough to overcome the electric field. The magnitude of the difference in these two cases corresponds to the factor of 3 difference in the charge-exchange reaction rate. The momentum transfer case has less ions being pulled back, because a substantial number of reactions lead to charge-exchange ions with sufficiently large axially directed velocities. Away from the thruster exit near the axis, the profiles are nearly identical for these cases as well as the $T_e = 5$-eV case.

Comparisons of velocity distribution functions of charge-exchange ions in the simulation are shown in Figs. 16–18 for the base and momentum transfer cases. Figure 16 shows the distribution

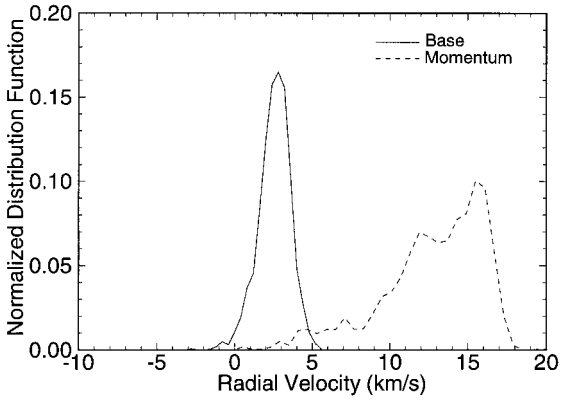

Fig. 18 Normalized velocity distribution functions of charge-exchange ions away from the beam ($r \approx 20$ cm), 45 cm away from the thruster exit plane.

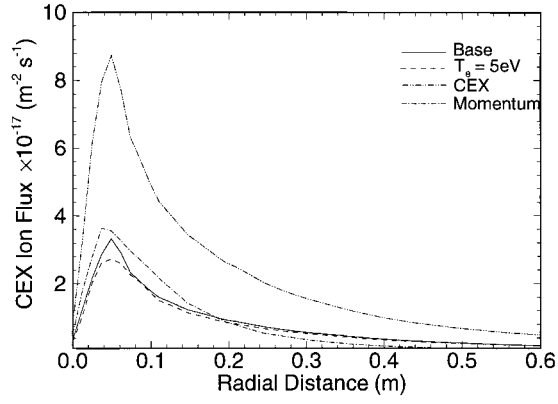

Fig. 19 Comparisons of charge-exchange ion flux in the radial direction 20 cm from the thruster exit.

of axial velocity at the beam edge 10 cm from the thruster exit. The base case merely forms charge-exchange ions with the distributions of the neutrals (both from the exit and the background). The thermal spread is quite low for both, as indicated by the sharp spike around zero velocity. The momentum transfer case shows a more uniform distribution between 0 and 35,000 m/s (the relative velocity of the collisions). Figure 17 shows the distribution of radial velocity at the same location. Again, the momentum case is more uniform. Also, the base case indicates acceleration of these ions because of electric fields. The shift of the peak shows an average velocity around 1000 m/s, whereas the thermal velocity is only about 250 m/s. This acceleration is more apparent in Fig. 18. This shows the distribution in a computational cell whose center is about 45 cm axially from the exit and 20 cm from the axis of symmetry. It shows a representative distribution away from the ion beam. The peak in the base case is again shifted by acceleration to an average of 2500 m/s, and has a wider spread than on the beam edge. The momentum transfer case also shows this acceleration as particles are biased toward a higher velocity. The axial velocity distribution at this location is similar to that shown in Fig. 16.

Figure 19 shows a radial profile of charge-exchange ion flux 20 cm from the thruster exit plane. The flux in the radial direction gives an indication of the depletion of charge-exchange ions from the ion beam. The cross-section case is higher than the base case, because the density is about three times higher. This is apparent from Fig. 20, which shows the radial velocity. The momentum transfer case shows how the postcollisional velocity of these charge-exchange ions is distributed isotropically. Its flux is comparable with the base case. The higher temperature case has a higher radial velocity than the base case, but the flux is nearly identical.

The backflow of charged particles may be harmful to spacecraft components, such as the solar arrays. A plot of total ion current density 10 cm behind the thruster exit (Fig. 21) shows the variation

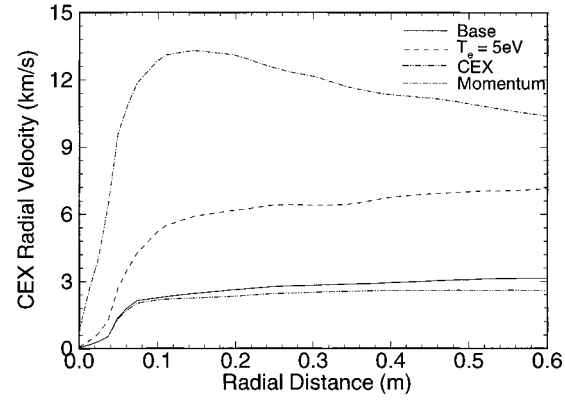

Fig. 20 Comparisons of charge-exchange ion radial velocity 20 cm from the thruster exit.

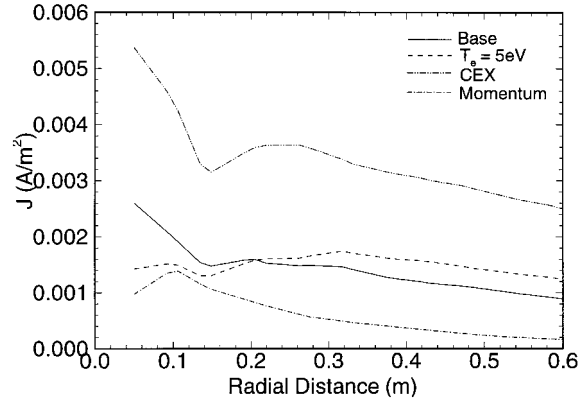

Fig. 21 Comparisons of total ion current density 10 cm behind the thruster exit.

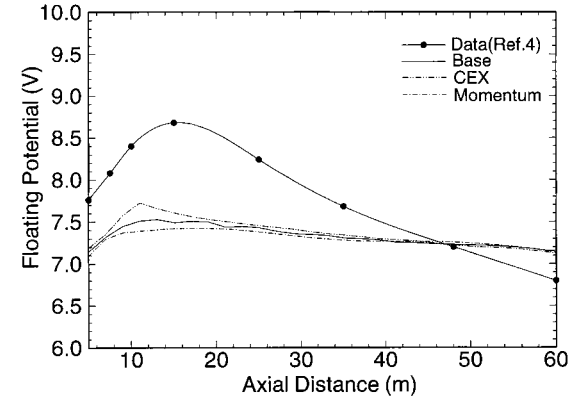

Fig. 22 Comparisons of floating potential along axis for various cases.

for the different cases. The cross-section case is the only one that is substantially different. This again shows the higher density of charge-exchange ions. These values are not the only concern for interaction with the spacecraft. The grid material sputtered by the charge-exchange ions may be ionized. These heavy metallic ions would then be affected by the electric fields created by the charge-exchange ions. Comparisons of electric field for these cases follow.

In Fig. 22, a comparison with experimental measurements of floating potential along the axis taken by de Boer[4] indicates reasonable agreement. The largest discrepancy is again a result of the lack of beam focusing. The simulation results are time averaged over 1000 time steps. In the actual simulations, these values vary with each time step. The agreement is sufficient to permit a reasonable estimate of the electric fields. A radial profile 30 cm from the

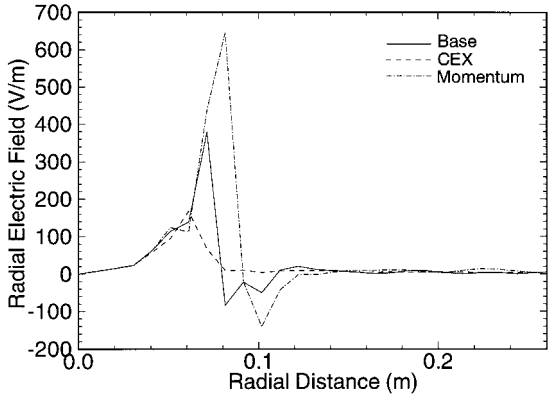

Fig. 23 Comparisons of radial electric field 30 cm away from the thruster exit.

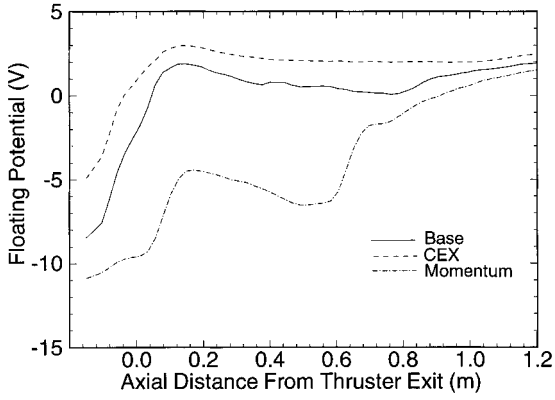

Fig. 24 Comparisons of potential 10 cm above the thruster.

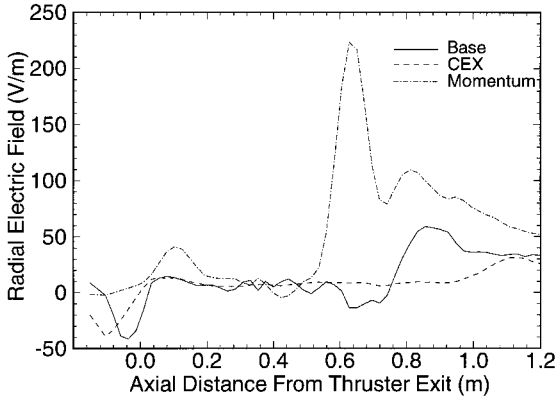

Fig. 25 Comparisons of radial electric field 10 cm above the thruster.

exit in Fig. 23 shows a strong radial electric field at the edge of the beam, where the gradients in charge density are most pronounced. Its magnitude is indicative of the beam thickness. The edge is well defined, because the beam ions are only moderately affected by the electrostatic forces. Further away from the axis, the field is nearly negligible. A plot of the axial electric field shows a similar trend and is not included. It indicates a strong field pulling ions behind the thruster at the edge of the ion beam. Figures 24 and 25 show the sensitivity of the potential and electric field to model assumptions. At a fixed radial position 10 cm above the thruster exit, the potential and radial electric field are compared for these cases. Figure 24 reflects the differences in ion density in these cases, because $\chi \sim \ell_n(n)$. The slope of the lines behind the thruster exit indicate the electric fields that accelerate the ions in the backflow region and toward the spacecraft. The magnitude of this axial electric field ranges from $\approx$10–30 V/m for these cases. Farther away from the axis, this field goes to zero. The values for potential are considerably lower than those found experimentally by Pollard,[5] even though the ion density values are comparable. The negative potential is an artifact of the Boltzmann relation. This discrepancy suggests that, away from the beam, the potential may not be defined by the Boltzmann relation. The radial electric field shown in Fig. 25 has more variation than the previous field in Fig. 23. The peaks are where the edge of the beam is encountered. These again are more pronounced for the momentum transfer case, because the charge-exchange ion density is lowest for this case.

Conclusions

A hybrid DSMC–PIC code was developed for the computation of plumes from ion thrusters and HCTs. Particles were used to simulate directly the properties of ions and neutral atoms. Both charge-exchange and momentum transfer collisions between neutrals and ions were included. Specification of a back pressure is included for simulation of laboratory experiments. An implicit grid scheme permitted a large number of PIC grid cells without inordinate memory costs. The two particle methods as well as their grids were maintained independently to allow modification of one without interfering with the other.

The code was applied to simulate the plume from the UK-10 ion thruster. The results compared satisfactorily with available experimental data for ion flux, ion density, and floating potential. These comparisons also indicated the significance of the initial ion velocity profile assumed in the computations. Computations where the acceleration grid was assumed to be a section of a sphere indicated that the ion beam, although altered noticeably, followed its initial profile in the near plume. The various uniform velocity simulations showed very little variation in this region. A better understanding of the trajectory of the ions between the screen grids is needed to determine their profile at the thruster exit more accurately. This profile is necessary to obtain better agreement with the experimental data.

The expected ion dynamics were captured qualitatively. The beam ions spread more as a result of the electric fields than they would because of purely thermal effects. The charge-exchange ions were pulled back toward the thruster near the exit and away from the beam farther away. The profile of the charge-exchange ions was found to be sensitive to various physical assumptions. Among these were electron temperature, background pressure, charge-exchange collision cross section, and the collision dynamics for charge-exchange reactions. Comparisons of ion density with experimental data indicated the significance of the charge-exchange cross section, particularly away from the ion beam. These comparisons also demonstrated that the change in momentum after charge-exchange collisions was less pronounced than that predicted by hard-sphere collisions. Computations that employed either hard-sphere collision dynamics for charge-exchange collisions or an increased electron temperature, underpredicted the ion density in comparison with experimental measurements. The sensitivity of the charge-exchange ions to these assumptions indicates a need for better understanding of these phenomena. Along the axis, the various computations gave potential values in reasonable agreement with experimental data. However, the potential in the plume away from the beam was underpredicted by these computations. This suggests that the Boltzmann relation does not accurately define the potential outside the beam.

Acknowledgments

Funding for this research was provided by NASA John H. Glenn Research Center at Lewis Field through Grant NAG3-1451. Eric Pencil was the Grant Monitor.

References

[1] Bird, G. A., *Molecular Gas Dynamics and the Direct Simulation of Gas Flows*, Oxford Univ. Press, Oxford, England, UK, 1994.

[2] Birdsall, C. K., and Langdon, A. B., *Plasma Physics Via Computer Simulation*, Adam Hilger, Bristol, England, UK, 1991.

[3] Fearn, D. G., Martin, A. R., and Smith, P., "Ion Propulsion Research and Development in the UK," *Journal of British Interplanetary Society*, Vol. 43, No. 10, 1990, pp. 431–442.

[4]de Boer, P. C. T., "Electric Probe Measurements in the Plume of an Ion Thruster," *Journal of Propulsion and Power*, Vol. 12, No. 1, 1996, pp. 95–104.

[5]Pollard, J. E., "Plume Angular, Energy, and Mass Spectral Measurements with the T5 Ion Engine," AIAA Paper 95-2920, July 1995.

[6]Roy, R. S., "Numerical Simulation of Ion Thruster Plume Backflow for Spacecraft Contamination Assessment," Ph.D. Dissertation, Dept. of Aeronautics and Astronautics, Massachusetts Inst. of Technology, Cambridge, MA, 1995.

[7]Wang, J., Brophy, J., and Brinza, D., "3-D Simulations of NSTAR Ion Thruster Plasma Environment," AIAA Paper 96-3202, July 1996.

[8]Rapp, D., and Francis, W. E., "Charge Exchange Between Gaseous Ions and Atoms," *Journal of Chemical Physics*, Vol. 37, No. 11, 1962, pp. 2631–2645.

[9]Pollard, J. E., "Profiling the Beam of the T5 Ion Engine," IEPC Paper 97-019, Aug. 1997.

[10]Boyd, I. D., VanGilder, D. B., and Liu, X., "Monte Carlo Simulation of Neural Xenon Flows in Electric Propulsion Devices," *Journal of Propulsion and Power*, Vol. 14, No. 6, 1998, pp. 1009–1015.

[11]Ruyten, W. M., "Density-Conserving Shape Factors for Particle Simulations in Cylindrical and Spherical Coordinates," *Journal of Computational Physics*, Vol. 105, 1993, pp. 224–232.

[12]Myers, R. M., Pencil, E. J., Rawlin, V. K., Kussmaul, M., and Oden, K., "NSTAR Ion Thruster Plume Impacts Assessments," AIAA Paper 95-2825, July 1995.

[13]Dietrich, S., and Boyd, I. D., "Scalar and Parallel Optimized Implementation of the Direct Simulation Monte Carlo Method," *Journal of Computational Physics*, Vol. 126, 1996, pp. 328–342.

[14]Oh, D., and Hastings, D., "Axisymmetric PIC-DSMC Simulations of SPT Plumes," IEPC Paper 95-160, Sept. 1995.

[15]Gatsonis, N. A., and Yin, X., "Axisymmetric DSMC/PIC Simulation of Quasineutral Partially Ionized Jets," AIAA Paper 97-2535, July 1997.

[16]Baganoff, D., and McDonald, J. D., "A Collision-Selection Rule for a Particle Simulation Method Suited to Vector Computers," *Physics of Fluids A*, Vol. 2, No. 7, 1990, pp. 1248–1259.